



HAL
open science

Ultrafast photoinduced flavin dynamics in the unusual active site of the tRNA methyltransferase TrmFO

Nadia Dozova, Fabien Lacomat, Charles Bou-Nader, Djemel Hamdane, Pascal Plaza

► To cite this version:

Nadia Dozova, Fabien Lacomat, Charles Bou-Nader, Djemel Hamdane, Pascal Plaza. Ultrafast photoinduced flavin dynamics in the unusual active site of the tRNA methyltransferase TrmFO. *Physical Chemistry Chemical Physics*, 2019, 21 (17), pp.8743-8756. <10.1039/C8CP06072J>. <hal-02095777>

HAL Id: hal-02095777

<https://hal.science/hal-02095777v1>

Submitted on 7 Dec 2020

HAL is a multi-disciplinary open access archive for the deposit and dissemination of scientific research documents, whether they are published or not. The documents may come from teaching and research institutions in France or abroad, or from public or private research centers.

L'archive ouverte pluridisciplinaire **HAL**, est destinée au dépôt et à la diffusion de documents scientifiques de niveau recherche, publiés ou non, émanant des établissements d'enseignement et de recherche français ou étrangers, des laboratoires publics ou privés.



HAL Authorization

Ultrafast photoinduced flavin dynamics in the unusual active site of the tRNA methyltransferase TrmFO

Nadia Dozova^a, Fabien Lacomat^a, Charles Bou-Nader^b, Djemel Hamdane^{b,*}, Pascal Plaza^{a,*}

^a PASTEUR, Département de chimie, École normale supérieure, PSL University, Sorbonne Université, CNRS, 75005 Paris, France.

^b Laboratoire de Chimie des Processus Biologiques, CNRS-UMR 8229, Collège de France, Sorbonne Université, 75005 Paris, France.

ABSTRACT

Flavoproteins often stabilize their flavin coenzyme by stacking interactions involving the isoalloxazine moiety of the flavin and an aromatic residue from the apoprotein. The bacterial FAD and folate-dependent tRNA methyltransferase TrmFO has the singularity of stabilizing its FAD coenzyme by an unusual H-bond-assisted π - π stacking interaction, involving a conserved tyrosine (Y_{346} in *Bacillus subtilis* TrmFO, *BsTrmFO*), the isoalloxazine of FAD and the backbone of a catalytic cysteine (C_{53}). Here, the interaction between FAD and Y_{346} is been investigated by measuring the photoinduced flavin dynamics of *BsTrmFO*, in the wild-type (WT) protein, C53A and several Y_{346} mutants by ultrafast transient absorption spectroscopy. In C53A, the excited FAD very rapidly (0.43 ps) abstracts an electron from Y_{346} , yielding the $FAD^{\bullet-}/Y_{346}OH^{\bullet+}$ radical pair, while relaxation of the local environment (1.3 ps) of the excited flavin produces a slight Stokes shift of its stimulated emission band. The radical pair then decays via a charge recombination, mostly in 3-4 ps, without any deprotonation of $Y_{346}OH^{\bullet+}$ radical. Presumably, the H-bond between Y_{346} and the amide group of C_{53} increases the pKa of $Y_{346}OH^{\bullet+}$ and slows down its deprotonation. The dynamics of WT *BsTrmFO* shows additional slow decay components (43 and 700 ps), absent in the C53A mutant, assigned to excited FAD_{ox} populations not undergoing fast photoreduction. Their presence is likely due to a more flexible structure of WT protein, favored by the presence of C_{53} . Interestingly, mutations of Y_{346} canceling its electron donating character lead to multiple slower quenching channels in the ps-ns regime. These channels are proposed to be due electron abstraction: (i) from the adenine moiety of FAD, a distribution of the isoalloxazine-adenine distance in the absence of Y_{346} explaining the multiexponential decay, or (ii) from the W_{286} residue, possibly accounting for one of the decays. This work supports the idea that H-bond-assisted π - π stacking controls TrmFO's active site dynamics, required for competent orientation of the reactive centers during catalysis.

1. INTRODUCTION

Flavins (FMN and FAD), which are derivatives of vitamin B2, are considered as the most versatile coenzymes in nature. They are used by flavoproteins as proton, electron, hydride, oxo or methylene transfer agents to catalyze a vast variety of biochemical reactions, mainly dependent on redox chemistry.^{1,2} One of the distinctive functional features of flavins is the diene moiety of their isoalloxazine ring, which allows them to cycle between three main redox states (oxidized, semi-reduced or fully reduced), each of them potentiality existing under various protonation states.³ Far beyond the reactivity of free flavins, it is actually the intimate and often synergistic interactions between the isoalloxazine and its apoprotein partner (ionic, hydrophobic or π - π stacking) that precisely regulate the physical and chemical properties of these coenzymes.⁴ It is thus important to characterize them, not only for fundamental mechanistic reasons, but also to address the challenges posed by the development of coenzyme-based artificial enzymes.⁵

In this regard, the flavoenzyme TrmFO, a FAD and folate-dependent bacterial tRNA methyltransferase,⁶⁻⁹ has recently been a model of choice for deciphering new, exquisite intermolecular interactions between flavin and apoprotein that allow TrmFO to achieve its unique chemical reactivity.¹⁰⁻¹⁴ While nearly all conventional DNA or RNA methyltransferases catalyze a direct CH₃-transfer using S-adenosyl methionine cofactor,¹⁵ TrmFO exhibits a complex multi-step mechanism wherein reduced FAD (FADH⁻) first mediates a CH₂-transfer from the 5,10-methylenetetrahydrofolate to tRNA via an unprecedented flavin iminium (FAD=CH₂) intermediate, and then reduces CH₂ to CH₃ by transferring a hydride.^{12,16} Since then, the unrelated flavoenzyme ThyX has been shown also to rely on the same intermediate to synthesize the DNA nucleotide dTMP in some bacteria and archaea,¹⁶⁻¹⁸ suggesting that the occurrence of this iminium species could be more widely spread in flavoenzyme reactivity than anticipated. Remarkably, in the absence of tRNA, TrmFO is able to store the otherwise reactive iminium intermediate in the form of a stable protein-FAD adduct via the formation of a covalent C-S bond with a conserved cysteine residue (C₅₃ in *Bacillus subtilis* TrmFO, noted *BsTrmFO*).¹² According to the crystal structure of *Thermus thermophilus* TrmFO (*TtTrmFO*),⁷ which shares 51% sequence identity with *BsTrmFO*, this cysteine (C₅₁ in *TtTrmFO*) lies on a flexible loop at the immediate vicinity of the FAD N5 nitrogen.

In the eager search for molecular phenomena that control the C-S bond formation/cleavage cycle, some of us uncovered the pivotal role of a π - π stacking interaction assisted by hydrogen bond in promoting proper FAD binding and structure of TrmFO's active site.¹⁴ This interaction involves three

key players: a conserved tyrosine (Y₃₄₆ in *BsTrmFO*), the isoalloxazine moiety and the backbone of C₅₃ (Figure S1).^{7,14}

Most interestingly, the fluorescence of TrmFO, arising from the oxidized FAD (FAD_{ox}), is strongly quenched in the wild-type (WT) and C53A proteins while it is much larger when Y₃₄₆ (Y₃₄₃ in *TtTrmFO*) is replaced by an alanine or phenylalanine.^{14,19} This quenching effect has been attributed to an efficient electron transfer (ET) from the stacked tyrosine to the flavin.¹⁹ Similar ET phenomena from aromatic amino acids (Tyr and Trp) to the excited isoalloxazine, resulting in ultrashort excited-state lifetimes, have been previously reported in numerous other flavoproteins.²⁰⁻³⁰ Such ET is very sensitive to the distance of the reactive centers and can reciprocally be considered as reporter of their relative position, as for instance formerly used to explore the structural flexibility of ThyX.³¹ Ultrafast spectroscopy is a particularly suited tool for probing such reactions, which Nag *et al.* recently applied to investigate the quenching dynamics of two variants of *TtTrmFO*, C51A and C51A/Y343F.¹⁹ They showed that upon excitation of FAD_{ox} at 390 nm, a very fast ET occurs from Y₃₄₃ to the excited FAD_{ox} in ~1 ps, yielding the flavin radical anion (FAD^{•-}) and the, formerly uncharacterized, protonated tyrosyl radical cation (Y₃₄₆OH^{•+}). This radical pair was then seen to recombine in ~3 ps, without apparent deprotonation of the tyrosyl cation. This constitutes a remarkable discovery in the field of photochemistry since YO^{•+} is usually considered an elusive species because of its extreme acidity (pK_a ~-2³²), favoring its ultrafast deprotonation.³² Upon replacement of Y₃₄₃ by a redox-inert phenylalanine, this ultrafast photoinduced reaction was inhibited. The same effect has been reported for other flavoproteins, as in flavodoxin.^{22,33} In the case of *TtTrmFO*, a slower and multiphasic decay of the excited state remained, which Nag *et al.*¹⁹ attributed to an alternative ET from the W₂₁₄ tryptophan to the excited flavin. Such type of ET indeed occurs in many other flavoproteins,^{21,26,34-36} but the electron density of W₂₁₄ is not visible in the *TtTrmFO* structures,⁷ raising uncertainties about its relative position with respect to FAD. Moreover, the corresponding tryptophan is absent from the *BsTrmFO* sequence,⁷ suggesting that this ET mechanism could be limited to the *Thermus thermophilus* enzyme.

In the present work, we have measured for the first time the photoinduced flavin dynamics of *BsTrmFO* in both the WT and the C53A mutant, by ultrafast transient absorption spectroscopy. Contrary to *TtTrmFO*, it is indeed possible to prepare WT-*BsTrmFO* samples containing a reduced fraction of methylene-FAD-protein adduct, thereby allowing the selective excitation of the FAD_{ox} by choosing a wavelength where the adduct absorbs much less than FAD_{ox}, here 475 nm. The comparison of WT and C53A is meant to evaluate the possible role of the C₅₃ residue on the FAD-Y₃₄₆ interaction and on the dynamics of TrmFO's active site, although the C53A mutation does not necessarily cancel the hydrogen bond between Y₃₄₆ and the backbone of C₅₃. In addition, several Y₃₄₆ single mutants of *BsTrmFO* (Y346A, Y346M and Y346F) were studied to investigate the

forementioned secondary quenching channels, in the absence of Y₃₄₆ and of any equivalent to the W₂₁₄ of *TtTrmFO*.

2. MATERIALS AND METHODS

2.1. Samples

Five variants of *BsTrmFO* (WT, C53A, Y346A, Y346M and Y346F[†]) were prepared as previously described.^{14,37} As previously observed,¹³ overnight exposure of freshly purified WT *BsTrmFO* to air significantly reduced the amount of reduced FAD-CH₂-C₅₃ adduct, which presents a maximum absorption around 360 nm,^{12,16} and completely removed the FAD-CH₂-C₅₃• radical, an inactive one-electron oxidized product of the latter adduct. The Y346 mutants were isolated from *E. coli* as apoproteins. To reconstitute the corresponding holoproteins, each freshly purified apoprotein was incubated with two equivalent of FAD_{ox} and the unbound flavin was then removed on a PD10 desalting column as detailed previously.^{14,16}

The steady-state absorption spectra of the samples used for transient absorption spectroscopy are provided in ESI, Section S2 (Figure S2). All *BsTrmFO* mutants essentially exhibit the characteristic bands of FAD_{ox},^{36,38-40} here situated around 375 and 445 nm. The WT spectrum additionally contains a contribution of the methylene-FAD adduct, around 360 nm. We estimated that the fraction of methylene-FAD adduct in our WT sample is of the order of 40 % and that, under excitation at 475 nm, the fraction of excited flavin in adduct form is limited to ~5 %, which can reasonably be neglected (see details in ESI, Section S2). In the case of 405-nm excitation, this fraction is however too large to be neglected (15 %); we therefore present only results on WT with excitation at 475 nm.

2.2. Transient absorption spectroscopy

Broadband transient absorption spectra were recorded by the pump-probe technique with white-light continuum probe, as previously described.⁴⁰ The pump beam was tuned at 475 nm with a noncollinear optical parametric amplifier (NOPA, Clark MXR) for most experiments. Complementary recordings were made under excitation at 405 nm, obtained by frequency doubling of the laser source beam in a BBO crystal.³⁹ It was checked by comparison with a reference sample of [Ru(bpy)₃]²⁺ complex^{41,42} that the fraction of excited molecules in the probed volume was about 4%, ensuring excitation in the linear regime. Experiments under 475-nm excitation were performed with polarized probe,³⁶ thereby allowing access to transient anisotropy data in addition to the standard isotropic

[†] The notation 'WT' will often be used as an abbreviation for 'wild-type *BsTrmFO*'. Similarly, 'C53A', 'Y346A', 'Y346M' and 'Y346F' alone will be used to refer to the different mutants of *BsTrmFO*.

transient absorption spectra (see below). The experiments under 405-nm excitation were performed at the magic angle configuration of pump and probe polarizations, which only provides isotropic spectra.³⁹

The samples were contained in 1-mm optical path quartz cells (width: 2 mm, containing ~60 μL) and kept at 10°C with a thermostated holder. The sample cell was continuously moved back and forth in horizontal and vertical directions to avoid exciting the same region consecutively. Steady-state absorption spectra of the samples were regularly recorded during the experiments to check that no sample degradation occurred.

The raw differential absorption spectra were first corrected from the chirp of the probe beam, which was independently measured by recording cross-phase modulation⁴³ (XPM) in the pure solvent. When available, the polarized transient spectra (ΔA_{\parallel} and ΔA_{\perp}) were replaced by the isotropic transient absorption spectra (ΔA_{iso}) and the transient anisotropy spectra (r), with the standard definitions of Equations 1 and 2. Note that the anisotropy based on transient absorption spectra is a complex quantity that may in particular diverge when the denominator (isotropic signal) vanishes. The individual contributions coming from the different transitions of the different involved species may formally be accounted for by a well-known addition rule.⁴⁴ This approach was however not employed in the present work and anisotropy was simply used at a qualitative level.

$$\left\{ \begin{array}{l} \Delta A_{\text{iso}} = \frac{1}{3}(\Delta A_{\parallel} + 2 \Delta A_{\perp}) \\ r = \frac{\Delta A_{\parallel} - \Delta A_{\perp}}{\Delta A_{\parallel} + 2 \Delta A_{\perp}} \end{array} \right. \quad \begin{array}{l} (1) \\ (2) \end{array}$$

Non-correctable scattering of the pump beam was masked in the transient spectra. The 405-nm excitation was in fact essentially used to displace the masked region and uncover the spectrum around 475 nm in the experiment with 475-nm excitation. The drawback is that an additional excess energy (3639 cm^{-1}) was given to the flavin molecules upon excitation at 405 nm.

2.3. Data analysis

Multiexponential global analysis with singular value decomposition⁴⁵ was performed simultaneously on the parallel and perpendicular spectra, as described previously.³⁶ Effective fits of the isotropic and anisotropy data were deduced from these fits with Equations 1 and 2. In the case of 405-nm excitation, simple analysis of the isotropic data was done.

The global fits are characterized by a series of time constants and associated pre-exponential factor spectra, called decay-associated difference spectra (DADS). The fits are however more conveniently summarized by the so-called evolution-associated difference spectra (EADS), which correspond to the states a virtual cascading model with 100% quantum yield between one state and the following

one.⁴⁶ When available, the polarized EADS were converted into isotropic EADS and evolution-associated anisotropy spectra (EAAS) with Equations 1 and 2.

It may be noted that in the above global analysis, all phenomena are decomposed into a sum of kinetic traces (exponentials) associated to time-independent spectra (DADS). This treatment hence does not explicitly treat the case of continuous shifting or deforming bands. To analyze this type of behavior, a specific analysis as to be devised, such as tracking the position and intensity of the maximum of a given band as a function of time (see 4.1.1).

3. RESULTS

3.1. Transient absorption spectroscopy of the wild-type *BsTrmFO*

A selection of isotropic transient absorption spectra of WT-*BsTrmFO*, recorded between 0.3 and 3.2 ns after excitation at 475 nm, are shown in Figure 1 (A-C).

At 0.3 ps (Figure 1A), the spectrum exhibits two negative bands peaking at 446 and 550 nm; the first one is dominated by ground-state bleaching (GSB) and the second one by stimulated emission (SE). Three positive bands dominated by transient absorption (TA) are also seen: at 365 nm with a minor shoulder around 400 nm (named TA₁), at 511 nm (TA₂) and from 600 to 750 nm (TA₃). These are typical features of excited FAD_{ox} (FAD_{ox}*) already reported for other oxidized flavoproteins^{26,36,40,47,48} and free FAD in solution.^{39,49}

From 0.3 to 1.8 ps (Figure 1A) the intensity of all bands decrease with the notable exception of the TA₂ band that increases until 0.9 ps before starting to decrease (Figure 1A). Simultaneously the TA₁ band decreases, more rapidly on its blue side (365 nm) than on its red side (400 nm), thereby acquiring a broader shape. The SE band concomitantly shifts to the red (to 559 nm) and its net negative part reduces to a small region, suggesting that it is overlapped with some strong transient absorption band.

From 1.8 ps to 22 ps (Figure 1B), the TA and GSB bands go on decaying with some changes of shape: the TA₁ band becomes narrower again and relatively more intense than the GSB and TA₂ bands. Concomitantly, the SE band broadens rather than decaying and its net negative part widens again.

After 22 ps, a spectrum resembling that of FAD_{ox}* slowly decays on the sub-ns timescale (Figure 1C). The shape of the TA₁ band further changes during this step, with the progressive reduction of the shoulder at 400 nm. A small residual spectrum is observed at 3.2 ns.

The transient absorption spectra were globally fitted by a sum of 5 exponentials followed by a plateau. The obtained time constants are: 0.38, 1.15, 4.1, 43 and 700 ps (Table 1). The corresponding isotropic DADS are given in ESI, Section S4.1 and the EADS in Figure 2A. Figure S5A in ESI, Section S5.1

shows the same spectra normalized at the maximum of their bleaching band, in order to better distinguish the changes of shape between them.

The initial excited-state decay takes place in 0.38 ps and 1.15 ps. During these steps, the EADS (Figure 2A; Figure S5A) clearly show the evolution of the TA₁ band (growth of the 400-nm shoulder), the shift of the SE band and the increase of the TA₂ band. The TA₂ band then decays in 4.1 ps, together with the TA₁ band whose shape changes again (reduction of the shoulder). During the remaining kinetic steps (43 ps, 710 ps), all bands decay but the relative intensity of the TA₁ and SE bands diminishes during the last phase. The final spectrum (plateau) exhibits a net negative SE band, indicating the persistence of a long-lived excited flavin population.

3.2. Transient absorption spectroscopy of the C53A mutant

Figure 1 (D-E) shows a selection of isotropic transient absorption spectra of the C53A mutant, recorded between 0.3 ps and 100 ps, after excitation at 475 nm. Globally, the behavior of C53A resembles that of WT but is in fact simpler, with fewer kinetic phases.

Like in the case of WT, the spectrum at 0.3 ps has the characteristic signature of FAD_{ox}^{*}, with a TA bands at 365, 506 and above 610 nm, a GSB band at 444 nm and a SE band at 550 nm. From 0.3 ps to 1.7 ps (Figure 1D) the spectral evolution is similar to that of WT: all bands decay except for TA₂ that on the contrary increases until 1.1 ps before starting to decrease. The TA₁ band becomes rounder and broader while the SE band shifts to 555 nm and only appears as a dip on a positive background, indicating that SE becomes dominated by TA in this region. A clear difference with WT appears from 1.7 ps to 22 ps (Figure 1E): the decay of the TA and GSB bands is here much more pronounced. The intensity of the GSB and TA₂ bands first increase relatively to that of the TA₁ and TA₃ bands. After 10 ps, no more changes of spectral shape are observed. A very small residual spectrum remains at 100 ps (Figure 1E-inset).

The transient absorption spectra of C53A could be fitted with a reduced sum of four exponentials, with time constants 0.30, 1.0, 3.0 and 9.3 ps (Table 1), followed by a plateau. The corresponding DADS are provided in ESI, Section S4.1. The EADS are presented in Figure 2B (normalized EADS are shown in Figure S5B of ESI, Section S5.1).

As well seen on the EADS, most of the initial excited-state decay occurs in 0.3 ps; it then goes on in 1.0 ps while the TA₂ band increases. The final decay of all bands in fact proceeds with two time constants: 3.0 ps and 9.3 ps. The very small plateau of the fit (inset in Figure 2B) accounts for the remaining signal observed at 100 ps. One may note a keen resemblance of EADS5 and EADS1, which suggests that the population responsible for the plateau is composed of excited flavins.

In order to reveal the spectral region masked by scattering of the pump beam (around 475 nm), additional experiments were performed with excitation at 405 nm (magic angle only; raw spectra not

shown). The isotropic spectra were satisfactorily fitted by the same model as above; the obtained time constants (see Table S1 in ESI, Section S3), as well as DADS (ESI, Section S4.2) and EADS (ESI, Section S5.2) are very similar to the ones obtained with excitation at 475 nm.

3.3. Transient absorption spectroscopy of the Y₃₄₆ mutants

Since the transient absorption behavior of the three studied Y₃₄₆ mutants (Y346A, Y346M and Y346F) are quite similar, only that of Y346A will here be described in details. Selected isotropic spectra of Y346A, recorded between 0.3 ps and 3.2 ns after excitation at 475 nm, are shown in Figure 3.

At 0.3 ps one observes the same characteristic features of FAD_{ox}* as previously detailed. The subsequent spectral evolution is however completely different, with a much slower amplitude decay accompanied by considerably smaller changes of shape. From 0.3 ps to 100 ps, one observes only a moderate decrease of most of the bands (the TA₂ band however remains approximately constant). The shape of the TA₁ band does not change but a shift of the SE band to 565 nm is observed. Between 100 ps and 3.2 ns, most bands decay more strongly (except TA₃), without shift of the SE band. The shape of the TA₁ band concomitantly changes, with a relative intensity increase of the shoulder at 390 nm.

The transient absorption data were fitted by a sum of three exponentials and a plateau. The time constants (4.0, 100, and 1600 ps) are recalled in Table 1, together with the close ones of Y346M and Y346F. The corresponding DADS may be found in ESI, Section S4.1 and the EADS in Figure 2C. The first three EADS are very similar in shape (see normalized EADS in Figure S5C), the main difference between them being the SE band that progressively shifts to the red; the concomitant relative increase of the TA₂ band is in fact likely the mere consequence of that shift (reduction of negative SE contribution). The excited-state decay is seen to be distributed over the three time constants, the last one being predominant. The last EADS (plateau) is quite different from the others: it features a larger shoulder at 390 nm and many changes in the relative intensities of the various bands. The presence of a marked dip in the SE region (around 567 nm) suggests that a sub-population of excited flavin remains in the ns timescale.

As seen in Figure 2(D-E), the EADS of Y346M and Y346F highly resemble those of Y346A. It may however be observed that the spectra of Y346M show larger variations, in particular in the TA₁ band below 400 nm. This effect is likely related to corresponding minor differences observed in the steady-state absorption spectra (Figure S2), assigned to a somewhat less rigid environment of FAD_{ox} in Y346M (ESI, Section S2). It is thus expected that the different GSB contribution slightly alters the transient absorption spectra. It is also possible that the same cause also mildly modifies the pure TA

and SE contributions, yielding the observed result. The overall dynamics of all Y_{346} mutants are however very similar and will be interpreted within the same framework (Section 4.3).

Upon excitation at 405 nm, the general behavior described above is also observed, with the notable difference that an additional very short time constant (0.4-0.6 ps depending on the protein) is necessary to fit the transient absorption spectra of all Y_{346} mutants. The time constants are provided in Table S1 of ESI, Section S3, and the corresponding DADS and EADS in ESI, Section S4.2 and ESI, Section S5.2, respectively.

3.4. Transient anisotropy

From all polarized experiments with excitation at 475 nm, transient absorption anisotropy spectra could be deduced with Equation 2 (not shown). The evolution-associated anisotropy spectra (EAAS) deduced from the global analysis of the data are presented in ESI, Section S6 (Figure S8).

In brief, the isotropic spectral evolutions described in the previous sections are also reflected at the anisotropy level. For WT and C53A, very large anisotropy changes accompany the fast excited-state decay, in particular in the SE region where the isotropic signal changes sign and crossing points ($\Delta A_{\text{iso}}=0$; hence diverging anisotropy) continuously change. It should be noted in the simpler case of C53A that EAAS3, associated to the first photoproduct following the decay of the excited state, exhibits a marked dip around 564 nm, curiously evoking the shape of a SE band as seen in isotropic spectroscopy. A similar feature has previously been described in the context of the flavin photoreduction of a class II photolyase⁵⁰ and assigned to small remnants of excited flavin population. We thus highly suspect such a contamination in the present case, and will return to this issue in the Discussion section (Section 4.1.3). We may finally observe that the final EAAS bears an interesting resemblance with the initial EAAS1 (especially marked for C53A), which supports the above-mentioned (Section 3.2) hypothesis that the plateau would be due to a small population of excited flavins.

As far as the Y_{346} mutants are concerned, one observes very little evolution of the anisotropy during the first two kinetic steps. Only minor changes related to the shift of the SE band (hence shift of the crossing points and associated anisotropy divergences) are observed. This pretty good invariance will be commented in Section 4.3.1. The main anisotropy changes are seen during the last kinetic step, in the ns timescale. Again, EAAS4 exhibits a more or less pronounced dip in the SE region, likely related to the persistence of a long-lived excited flavin population. This issue will be discussed further in Section 4.3.2.

4. DISCUSSION

4.1. Ultrafast dynamics of C53A

Since the transient absorption behavior of the C53A mutant of *BsTrmFO* turned out to be simpler than the one of the WT protein, the former will be discussed first. The additional dynamic features of WT will be commented in Section 4.2.

4.1.1. Charge separation

The transient absorption behavior of C53A (Section 3.2) clearly shows that the flavin excited state very rapidly decays to form a new product. This process is characterized by the disappearance of the SE band and the growth of a TA band around 500 nm (more completely seen with excitation at 405 nm; ESI, Section S5.2). Since this spectral dynamics is completely inhibited in the case of all studied Y_{346} mutant (Section 0), the predominant role of the electron donating character of Y_{346} in this reaction is established.

Following the same analysis previously developed by Nag *et al.* for the C51A mutant of *TtTrmFO*,¹⁹ it appears extremely likely that the excited flavin gets reduced to $FAD^{\bullet-}$ by Y_{346} . The high rate of the reaction is readily explained within the Marcus electron transfer (ET) theory^{51,52} by the very short distance between Y_{346} and FAD (2.7 Å; Figure S1) and their stacked configuration. It may furthermore be deduced that the produced tyrosyl radical is most probably still protonated (and here noted $Y_{346}OH^{\bullet+}$) because the 500-nm photoproduct band does not match the well-known spectroscopic signature of deprotonated tyrosyl radical (YO^{\bullet}), which exhibits a weak absorption band around 405 nm.^{53,54} One may indeed check with the example of an animal-like cryptochrome that a typical transient absorption spectrum of the $FAD^{\bullet-}/YO^{\bullet}$ radical pair is pretty flat in the 500-nm region,⁵⁵ and does not resemble the specific shape of EADS3. As noted by Nag *et al.*,¹⁹ the observation of the $YOH^{\bullet+}$ radical is exceptional because this species is known to be extremely acidic ($pK_a \sim -2$ ³²) and therefore expected to deprotonate rapidly. One may think that its observation in TrmFO is permitted by the very high rate of its formation. It may additionally be hypothesized that the particular H-bond between Y_{346} and the amide group of C_{53} stabilizes the protonated tyrosyl radical, increasing its pK_a and thereby slowing down its deprotonation.

It is interesting to emphasize that the photoreduction of the flavin is biexponential (0.30 and 1.0 ps) whereas a single exponential of 1.1 ps was reported by Nag *et al.* for the C51A mutant of *TtTrmFO*.¹⁹ It may further be noted that DADS1 and DADS2 (ESI, Section S4.1, Figure S3B) have very different shapes which allows us to rule out the possibility that the two fast components would correspond to two populations of the protein (*e.g.* characterized by different FAD- Y_{346} distances) undergoing the same ET process at different rates. We rather believe that they are two phases of the same process.

Inspection of the normalized EADS (Figure S5B) reveals that the first phase consists in a partial decay of the SE band, accompanied by a small red shift (~ 5 nm) of the latter. The 500-nm band concomitantly starts to rise and the 400-nm shoulder to grow. The second phase sees the final decay of the SE band and growth of the 500-nm band. To explain this behavior, we propose that the ET from Y_{346} to FAD_{ox}^* is in fact coupled to a fast relaxation of FAD_{ox}^* , due the response of the flavin environment (protein residues or nearby water molecules) to the change of charge distribution induced by the excitation.⁵⁶⁻⁵⁹

Within this interpretation, we intended to separate the two phenomena by tracking the spectral position and the intensity of the maximum of the SE as a function of time. We found that both curves could be fitted by a single exponential decay (Figure 4): the red shift dynamics is characterized by a time constant of 1.3 ps, while the pure excited-state decay, hence the flavin reduction, takes place in 0.43 ps (this time constant is noted in the simplified reaction Scheme 1). This fast coupled dynamics was interestingly not reported for *TtTrmFO*,¹⁹ which may tentatively be related to the fact *Thermus thermophilus* is a thermophile organism and that *TtTrmFO* is likely more rigid than *BsTrmFO*.⁶⁰ This extra rigidity might in turn be thought to reduce the response of the flavin environment to the optical excitation. It may further be noted that the rate of flavin reduction of *BsTrmFO* deduced from the above analysis (2.7 ps^{-1}) is significantly faster than the one of *TtTrmFO* (0.91 ps^{-1}). This difference (factor of 2.6) could be due to the slightly smaller FAD- Y_{346} distance in *BsTrmFO* (2.7 \AA) than in *TtTrmFO* (3.3 \AA according to PDB entry 3G5S⁷). For illustrative purpose only, let us mention that Page *et al.*'s empirical formula for Marcus ET⁵² (see details in Section 4.3.1) predicts a decrease of the rate constant by a factor of ~ 2.3 if the distance is increased by 0.6 \AA (all other factors being held constant), in qualitative agreement with the experimental values. This estimation is however to be taken with precaution because: (i) of the uncertainty on the FAD- Y_{346} distance, only obtained from a homology model in *BsTrmFO* and (ii) of the fact that for extremely fast ET, the above formula (exponential decay of the rate with distance) might not be valid, as recently discussed for other flavoproteins.^{28,30,61}

4.1.2. Charge recombination

Following the initial charge separation described above, the analysis of Section 3.2 shows that all photoproduct bands rapidly decay, with time constants of 3.0 and 9.3 ps. The residual spectral remaining after this decay (DADS5) is so small that it can for now be neglected. It can therefore be deduced that the $FAD^{\bullet-}/Y_{346}OH^{\bullet+}$ radical pair undergoes charge recombination during these phases, yielding the restoration of the starting oxidized flavin configuration. The biexponential nature of this process is specific to *BsTrmFO* as a single component of 3.0 ps was reported for *TtTrmFO*.¹⁹

Careful inspection reveals that DADS3 and DADS4 have quite similar shapes, although some differences may be distinguished (slightly different position of the bleaching band, different relative intensity of the 500-nm band). One could first conceive that these two kinetic components correspond to two distinct populations, undergoing charge recombination at slightly different rates, possibly because of some minor structural differences, also justifying the difference of shape of DADS3 and DADS4. Within this hypothesis, the population decaying in 3.0 ps would be dominant, representing about 84% of the total decay (fraction measured in the 380-nm band; this time constant is noted in the simplified reaction Scheme 1). It might alternatively be considered that charge recombination restores the flavin in a hot ground state, as recently reported for semi-reduced flavodoxin,⁶² and that the altered absorption spectrum of hot FAD_{ox} contributes to DADS4. However, since DADS4 retains a high similarity with DADS3, it is unlikely that the fourth kinetic step can be assigned to ground-state cooling alone. Charge recombination must still be the major contributor to it. We rather favor a third hypothesis, along which the spectroscopic signature of the FAD^{•-}/Y₃₄₆OH^{•+} pair would continue to evolve during the recombination process, possibly due to the response of the protein environment to the new charge distribution or to some cooling process of the radical pair, initially produced in a hot vibrational state as earlier proposed for a plant cryptochrome²⁶ and a (6-4) photolyase.³⁶

It may finally be mentioned that deprotonation of the Y₃₄₆OH^{•+} radical does not take place during the 3.0-ps and 9.3-ps steps as the characteristic spectrum of FAD^{•-}/YO[•],⁵⁵ with weak and flat profile above 500 nm, is not observed here. As mentioned above, it may be speculated that Y₃₄₆OH^{•+} is in fact stabilized by the unusual H-bond between Y₃₄₆ and the amide group of C₅₃, which would slow down the expected fast deprotonation of this radical.

4.1.3. Corrections to EADS3 and EADS4

We will next intend to extract from EADS3 and EADS4 the pure spectrum of the FAD_{ox} radical pair. This operation will be best performed with the EADS obtained with excitation at 405 nm (see ESI, Section S5.2), because the spectra are better defined in the critical region around 500 nm. In addition, the missing data around 405 nm may be rather well be filled by a straight line without much loss of information (*e.g.* compare Figures S5B and S7A). Let us however first mention two difficulties that need to be solved before proceeding to any calculation.

In the first place, the weak plateau observed at long pump-probe delays contributes by construction to all EADS. In order to focus on the species undergoing fast dynamics, EADS5 was subtracted from all EADS, yielding so-called EADS' (numbered from 1 to 4) as shown in Equation 3.

$$\begin{cases} \text{EADSi}' = \text{EADSi} - \text{EADS5} & (3) \\ \text{EADSi}'' = \text{EADSi}' - \alpha_i \text{EADS1}' & (4) \end{cases}$$

The second issue is the presence of a dip, evoking the shape of a SE band, in the anisotropy spectra EAAS3 and EAAS4 (with 475-nm excitation; Figure S8B). To check whether this comes from remnants of excited flavin population, a variable fraction of EADS1' was subtracted from EADS3' and EADS4', as shown in Equation 4. Factor α should be interpreted the fraction of the initial population remaining in the excited state. This operation was done for both polarizations (with the same factor α_i) and corrected anisotropy spectra (noted EAAS'') were calculated from the results with Equation 2. We found that the dip could be satisfactorily suppressed with $\alpha_3=0.07$ and $\alpha_4=0.02$ (Figure 5). With this choice, EAAS3'' and EAAS4'' adopt a similar shape, with a smooth variation of the anisotropy between 500 and 700 nm, which likely reflects the transition from a region where both $\text{FAD}^{\bullet-}$ and $\text{YOH}^{\bullet+}$ species contribute to a region where only $\text{FAD}^{\bullet-}$ contributes, without interference from FAD_{ox}^* . The corresponding EADS'', shown in Figure 6A, have also a smoother shape between 500 and 700 nm and one can observe that a shallow depression in the SE region has been compensated. It is however obvious that such a compensation could not have been made with the EADS alone. Only do the EAAS provide the sufficient sensitivity to reveal the minor FAD_{ox}^* population.

Given that polarized experiments were not available with excitation at 405 nm, we assumed that the same fraction of the initial excited state remained in EADS3 and EADS4 and the latter spectra were corrected with the same choice of α parameters as above. The results, similar to the previous case, are shown in Figure 6B.

A view of the same corrected EADS, arbitrarily normalized around 385 nm is provided in ESI, Section S7. Figure S9B in particular illustrates the clear difference of shape of EADS3'' and EADS4'', with relatively more pronounced and blue shifted peaks at 438 and 490 nm for EADS4''.

4.1.4. Spectrum of the radical pair

To extract a pure spectrum of the $\text{FAD}^{\bullet-}/\text{Y}_{346}\text{OH}^{\bullet+}$ radical pair, we used the standard decomposition of the relevant difference spectrum (ΔA_{rp}) into the sum of Equation 5, where c_{rp} is the concentration of radical pair, the ϵ_i are the molar absorption coefficients of the different species and L is the optical path. The $\epsilon_{\text{YOH}^{\bullet+}} + \epsilon_{\text{FAD}^{\bullet-}}$ spectrum then follows from bleaching compensation as shown in Equation 6.

$$\left\{ \begin{array}{l} \Delta A_{\text{rp}} = c_{\text{rp}}(\epsilon_{\text{FAD}^{\bullet-}} + \epsilon_{\text{YOH}^{\bullet+}} - \epsilon_{\text{FAD}_{\text{ox}}^*})L \\ \epsilon_{\text{YOH}^{\bullet+}} + \epsilon_{\text{FAD}^{\bullet-}} = \frac{\Delta A_{\text{rp}}}{c_{\text{rp}}L} + \epsilon_{\text{FAD}_{\text{ox}}^*} \end{array} \right. \quad (5)$$

$$(6)$$

To evaluate Equation 6, it is straightforward to get the $\epsilon_{\text{FAD}_{\text{ox}}^*}$ spectrum by normalizing the absorption spectrum of the protein (see ESI, Section S2). The choice of c_{rp} is however more critical and depends on the ΔA_{rp} spectrum taken for the calculation.

Using EADS3'', it is reasonable to assume that the quantum yield of radical pair formation at that kinetic step is one, because of the extreme rapidity of the charge separation process (0.43 ps). We

can thus take the initial excited state concentration as an estimate of c_{rp} . In turn, c^* was estimated to 10.9 μM using the transient spectra of the $[\text{Ru}(\text{bpy})_3]^{2+}$ complex recorded under the same conditions, as previously detailed.⁶³ The obtained spectrum (blue line in Figure 7; called for short RP_3) should of course be taken with some care but we note that changing c_{rp} by $\pm 20\%$ did not alter much the overall shape of the spectrum. Two bands may be seen: the one peaking at 377 nm is assigned to $\text{FAD}^{\bullet-}$ and the one at 445 nm to $\text{Y}_{346}\text{OH}^{\bullet+}$. We believe it is not reliable to go further and extract a pure spectrum of $\text{Y}_{346}\text{OH}^{\bullet+}$ because the absorption spectrum of $\text{FAD}^{\bullet-}$ is not known in TrmFO. One has thus to use a spectrum taken from another flavoprotein, as done by Nag *et al.* for *Tt*TrmFO.¹⁹ Different choices were tested⁶⁴⁻⁶⁶ (one example is provided in ESI, Section S9 for illustrative purpose) but very incomplete compensations were obtained below 420 nm (yielding unphysical negative values), which suggests that the spectrum of $\text{FAD}^{\bullet-}$ for *Bs*TrmFO has specific spectral features, possibly exhibiting a much less prominent sub-peak around 400 nm than in other proteins.⁶⁴⁻⁶⁶ It may just be mentioned that, since the absorption spectrum of $\text{FAD}^{\bullet-}$ is generally of relative lower amplitude between *ca.* 420 and 490 nm and in some cases quite flat,^{65,66} the maximum we observe at 445 nm may be close to that of the pure $\text{Y}_{346}\text{OH}^{\bullet+}$. A much more red-shifted maximum (490 nm) was however reported by Nag *et al.* for *Tt*TrmFO.¹⁹ Such a red maximum could also have been obtained in the present case, but at the cost of a much reduced c_{rp} , hardly compatible with our estimation of c^* , and of visible negative features due to incomplete bleaching compensation.

Taking EADS4" as starting difference spectrum is a more difficult task because a large amount of charge recombination has already taken place at that step. We therefore adjusted c_{rp} so as to produce a spectrum of similar shape as RP_3 . With a value of 2.1 μM , RP_4 was obtained (red line in Figure 7). Even if this spectrum is somewhat arbitrary, it should be mentioned that no choice of c_{rp} led to exactly identical RP_3 and RP_4 . The band of RP_4 around 450 nm systematically tends to have a different shape; with our choice of c_{rp} , it appears both slightly red-shifted and slightly narrower. We propose that this spectral change is related to a relaxation the $\text{Y}_{346}\text{OH}^{\bullet+}$ radical during the recombination process, either due to the response of its immediate environment or to vibrational cooling (as evoked in Section 4.1.2).

The 445-nm band in the RP spectra of Figure 7 bears a remarkable similarity with the broad absorption spectrum of the radical cation of 2,6-di-*tert*-butyl-4-methylphenol ($\text{ArOH}^{\bullet+}$),⁶⁷ which is centered at 450 nm in a glassy matrix of Bu^sCl at 77 K. It is worth noting that the corresponding spectrum of ArO^{\bullet} at 107 K has a much narrower peak at 401 nm.⁶⁷ The same trend has been observed for phenol in a frozen matrix argon, with a band of the radical cation ($\text{PhOH}^{\bullet+}$) at 423 nm while the deprotonated radical (PhO^{\bullet}) has a narrow peak at 396 nm.⁶⁸ Similarly, the radical cation and neutral radical of 4-methoxyphenol were reported at 440 and 410 nm, respectively.⁶⁹ These comparisons globally support our assignment of the 445-nm band to $\text{Y}_{346}\text{OH}^{\bullet+}$.

4.1.5. *Slowly decaying species*

To conclude the examination of the C53A results, let us recall that a very weak plateau (EADS5) remains after decay of all the fast components. In the experiment with excitation at 475 nm, EADS5 has the typical spectral signature of excited FAD_{ox} (insert of Figure 2B). It makes then sense to assume that a small fraction (about 1%) of the initial excited population does not undergo ultrafast charge transfer, possibly because of a larger distance between FAD and Y_{346} , and therefore decays much more slowly. This interpretation agrees well with the resemblance of the corresponding anisotropy spectrum, EAAS5, with the initial one, EAAS1, which is clearly assigned to FAD_{ox}^* . With excitation at 405 nm, the signature of EADS5 is not so clear (Figure S6A) but the signal-to-noise ratio of this experiment is somewhat worse. In the absence of more decisive contradictory proof, we tentatively maintain our interpretation that the plateau is due to a small population of slowly decaying excited flavin.

The corrections of EADS3' and EADS4' made in Section 4.1.3 also revealed the existence of a minor population of excited flavin (fraction α) that decays more slowly than the main part. This additional population is actually distinct from the one of the plateau because EADS5 was subtracted from all other EADS (Equation 3) before the correction. Since the global fit could not separate it from the components assigned to charge recombination, and as α substantially decreases from EADS3' to EADS4', it may be inferred that this minor population likely decays in a few ps, instead of 0.43 ps for the main decay. It therefore appears that a distribution of FAD species coexists, characterized by different excited-state lifetimes. This may be related to a some moderate flexibility of the active site of *BsTrmFO*, evoking (without reaching the same large extent) the conformational heterogeneity of the aforementioned thymidylate synthase *ThyX*.³¹ *ThyX* indeed exhibits a wide distribution of the distance between FAD and a nearby tyrosine residue (Y_{91}), resulting in a highly multiphasic fluorescence decay.

4.2. Ultrafast dynamics of WT

As mentioned above, the ultrafast dynamics of WT is quite similar to that C53A, the first three time constants (Table 1) and DADS (Figure S3) being close. The same conclusions drawn above for C53A relative to sub-ps charge separation, coupled to excited-state relaxation, and subsequent ps charge recombination are thus still fully applicable to WT.

It is however clear from the anisotropy data that the contribution of FAD_{ox}^* to EAAS3 (negative dip in the SE region) is much larger for WT than for C53A (Figure S8). A correction such as the one made for C53A (Section 4.1.3) may also be performed but with a much larger fraction of FAD_{ox}^* (~25%; not shown). At the next kinetic step, the weight of the FAD_{ox}^* population becomes so large that EADS4 can no longer be associated to charge recombination. It is rather assigned to the decay of some

FAD_{ox}* population, in 43 ps. The same assignment is further done for EADS5 (700 ps) and EADS6 (plateau). The presence of this multiplicity of FAD_{ox}* populations, decaying with different lifetimes, indicates that the heterogeneity of WT is significantly more pronounced than that of C53A. It cannot even be excluded that the actual distribution of FAD_{ox}* populations is in fact continuous, with major peaks as defined by our discrete multiexponential analysis. This result agrees with our previous structural biophysical studies of *BsTrmFO* showing that the wild-type protein is indeed more flexible than the C53A mutant,^{7,11} probably because the active site cysteine plays an important role in the dynamics of the active site loop in the vicinity of FAD. This flexibility of the active site loop is likely required to allow the nucleophilic attack of the catalytic intermediate FAD=CH₂ by C₅₃ in the absence of tRNA. Let us note that the "slow" FAD_{ox}* species are only revealed by the decay of a FAD_{ox}* difference spectrum. The nature of this decay is in fact not apparent as no intermediate, such as a FAD^{•-}/YOH^{•+}, is evidenced. One may just assume that the same quenching mechanism, involving reduction of the excited flavin by Y₃₄₆ followed by charge recombination, is at work in all case but the rates are modulated by the variations of distance between FAD and Y₃₄₆. The absence of any visible reaction intermediate suggests that charge recombination somehow becomes faster than charge separation for the slow species.

4.3. Multiexponential decay of the Y₃₄₆ mutants

The following discussion is centered on the Y346A mutant of *BsTrmFO* but, since the transient absorption behaviors of Y346M and Y346F are very similar to that of Y346A (Section 3.3), the conclusions drawn below are applicable to all three Y₃₄₆ mutants.

4.3.1. Nature of the deactivation channel

We have seen that the Y346A mutation inhibits the major, ultrafast, quenching pathway of *BsTrmFO* by photoinduced ET from Y₃₄₆ to the flavin. As previously observed for *TtTrmFO*,¹⁹ the replacement of Y₃₄₆ by a redox inert residue however does not cancel all deactivation channels. Instead of observing a very slow decay in the ns range, as expected for FAD in extended configuration^{3,39,70} or riboflavin,⁴⁹ a multiphasic decay including components as short as 4 ps is observed for all Y₃₄₆ mutants we studied (Table 1). A similar behavior was reported for the *TtTrmFO* C51A/Y343F double mutant.¹⁹ This fact reveals the existence of additional deactivation channels, not involving Y₃₄₆. It should additionally be mentioned that the decay of the Y₃₄₆ mutants is obviously coupled to a relaxation of the excited state, revealed by the conspicuous red shift of the SE band (Figure 3).

Like in the case of the initial flavin reduction of C53A (Section 4.1.1), we tried to separate the two phenomena by tracking the spectral position and the intensity of the maximum of the SE band as a

function of time. Both curves (Figure S10 in ESI, Section S8) needed a sum of three exponentials to be properly fitted. The time constants obtained for the shift dynamics: are: 3, 30 and 350 ps with similar amplitudes (see Table S2). The amplitude decay is characterized by time constants of 21, 240 and 2180 ps (with relative amplitudes of 6%, 22% and 72%, respectively). This analysis shows that the short time constant of the global analysis (4 ps) is in fact related to the shift dynamics while the long time constant (1600 ps) is essentially due to the amplitude dynamics, hence to the decay of the excited-state population.

Two hypotheses may be considered to explain the behavior of Y346A. It could first be speculated that the substitution of Y₃₄₆ by other residues disrupts the stacking interaction with the isoalloxazine ring and allows this moiety to move more freely and adopt different configurations. It is on the other hand known that the excited-state lifetime of FAD_{ox} in solution highly depends on the distance between the isoalloxazine and adenine moieties, with a fast decay (5-9 ps; attributed to isoalloxazine-to-adenine electron transfer) in stacked form and a slow decay (2-3 ns) in extended form.^{3,39,70,71} The present multiphasic population decay could then be related to the existence of a distribution of the isoalloxazine-adenine distance in the ground state, before excitation. The shorter distances (stacked-like configurations) could for instance be responsible for the fastest decay component (21 ps). It may be rather safely ruled out that a movement of the isoalloxazine takes place during the decay, *e.g.* increasing the distance and favoring slower decays, because the transient anisotropy measured in the TA, GSB and SE bands remain nearly constant during most of the process (Figure S8C). The hypothesis of a ground-state distribution of isoalloxazine-adenine distance might additionally explain the quite slow SE shift dynamics if the different populations had different local environments (more or less exposed to water molecules of the buffer) and thus different positions of their SE band.

Alternatively, it may be hypothesized that secondary electron donors would be responsible of additional deactivation channels by ET. In the same context, Nag *et al.*¹⁹ considered for *TtTrmFO* the role of W₂₁₄, located on a flexible loop close to the flavin. The flexibility of this loop was suggested to explain the multiphasic decay, as in the case of *ThyX*.³¹ However, W₂₁₄ is not conserved in *BsTrmFO* and the closest electron donor is W₂₈₆, situated on a α -helix at 8.2 Å from the isoalloxazine moiety of FAD (see Figure S1). Again for illustrative purpose, we estimated the impact of this rather large distance, the ET rate (k_{ET}) with Page *et al.*'s formula, here reproduced:⁵²

$$\log k_{ET} = 13.0 - (1.2 - 0.8\rho)(R - 3.6) - 3.1(\Delta G^0 + \lambda)^2/\lambda \quad (7)$$

Using $R = 8.2$ Å, $\Delta G^0 = -0.7$ eV (typical reduction potentials of excited FAD_{ox} and tryptophan in a photolyase were taken from Ref.³⁵), $\lambda = 1$ eV and $\rho = 0.76$ (standard values taken from Ref.⁵²), Equation 7 yields a time constant of the order of 100 ps. It is thus possible that W₂₈₆ would be responsible for the intermediate decay time (240 ps). It is more difficult to explain the 21-ps decay

with the same cause because W_{286} is not located in a particularly flexible position and large variations of its distance to FAD are unlikely. It is also hard to conceive that this deactivation channel would not drain completely the excited-state population and leave a large fraction of it decaying in the ns regime (2180 ps).

For the reasons just exposed, we tentatively favor the first hypothesis, based on a static distribution of the isoalloxazine-adenine distance after disruption of the stacking with Y_{346} . This interpretation would in turn confirm that Y_{346} plays a crucial role to anchor FAD in the extended configuration, and keeps it in a suitable position to perform its role in the enzymatic activity of TrmFO, as previously discussed.¹⁴ We however do not rule out the possibility that ET from W_{286} to the excited flavin could also contribute to the decay of Y_{346} . A specific follow-up study on the Y_{346A}/W_{386F} double mutant (scheduled in the near future) would likely decide on this specific matter.

4.3.2. Nature of the plateau

We finally discuss the spectral change occurring in the final kinetic phase of all Y_{346} mutants. As the normalized EADS clearly show (Figure S5C), the shape of the plateau is significantly different from all preceding EADS. This is readily explained by the formation of a new photoproduct, which we propose to be the triplet state of the flavin (noted $FAD_{ox}^{T_1}$). It is indeed known that the triplet state of flavins in solution^{72,73} or bound to different proteins^{23,72-76} is formed in the ns regime with relatively high quantum yields (up to 0.60 for phototropin⁷³). It is however obvious that the SE band of the excited singlet of FAD_{ox} (here noted $FAD_{ox}^{S_1}$ for clarity) is still present in EADS4 (negative dip around 565 nm), overlapped by a dominant positive background. We therefore propose that EADS4 is a superposition of contributions of both $FAD_{ox}^{S_1}$ and $FAD_{ox}^{T_1}$.

To support this hypothesis, a variable fraction of EADS3 was subtracted from EADS4 (Equation 8), so as to obtain a spectrum matching approximately the shape of published difference spectra of triplet flavin.^{75,76}

$$EADS4' = EADS4 - \alpha EADS3 \quad (8)$$

Figure 8 shows that a suitable choice of α makes EADS4' highly resemble published transient absorption spectra of the triplet state of different flavoproteins (phototropin from *Avena sativa* (LOV2 domain)⁷⁶ and AppA from *Rhodobacter sphaeroides* (BLUF domain)⁷⁵). EADS4' is thus assigned to $FAD_{ox}^{T_1}$. The superposition of contributions of both $FAD_{ox}^{S_1}$ and $FAD_{ox}^{T_1}$ in EADS4 means that the global fit was not capable of completely separating the slowest decay of $FAD_{ox}^{S_1}$ from the rise of $FAD_{ox}^{T_1}$, likely because this reaction takes place in the ns regime and our observation window is limited to 3.2 ns.

5. CONCLUSION

In the present work, we have measured the photoinduced flavin dynamics of *BsTrmFO*, both in wild-type and C53A proteins, by ultrafast transient absorption spectroscopy. We have shown that the selective excitation of FAD_{ox} in both cases leads to the ultrafast formation of the $\text{FAD}^{\bullet-}/\text{Y}_{346}\text{OH}^{\bullet+}$ radical pair. The biexponential dynamics of this reaction (about 0.35 and 1.1 ps in both proteins) is attributed to the coupling of the pure electron transfer reaction with the response of the local environment upon flavin excitation. Both phenomena could be separated in C53A, yielding a time constant of 0.43 ps for the pure flavin reduction and 1.3 ps for the excited flavin relaxation. The faster rate of ET in *BsTrmFO* than in *TtTrmFO* (1.1 ps¹⁹) could be due to a slightly shorter distance between FAD and Y_{346} in *BsTrmFO* (2.7 vs. 3.3 Å). The excited flavin relaxation dynamics, which was not reported in *TtTrmFO*, is here tentatively explained by the somewhat less rigid structure of *BsTrmFO* as compared to *TtTrmFO*, which comes from a thermophile organism. The absorption spectrum of the $\text{FAD}^{\bullet-}/\text{Y}_{346}\text{OH}^{\bullet+}$ radical pair, corrected from the ground-state bleaching contribution, is proposed (Figure 7). This radical pair decays via a charge recombination, mostly in 3-4 ps. An additional decay component of 9.3 ps is detected in the case of C53A, possibly due to the response of the protein environment to the charge distribution of the radical pair or to vibrational cooling of the latter. Remarkably, the $\text{Y}_{346}\text{OH}^{\bullet+}$ radical does not deprotonate prior or during the recombination process as expected from its high acidity. We hypothesized that this could be due to the H-bond between Y_{346} and the amide group of C_{53} , which would increase the pKa of $\text{Y}_{346}\text{OH}^{\bullet+}$ and slow down its deprotonation. Compared to the C53A mutant, the dynamics of wild-type *BsTrmFO* shows additional slow decay components (43 and 700 ps, larger plateau) that are assigned to non-negligible populations of excited FAD_{ox} not undergoing fast photoreduction. This result agrees well with more flexible structure of WT as compared to C53A, likely due to the role played by C_{53} in the dynamics of the active site loop.^{7,11}

On the other hand, three point mutants of Y_{346} (Y346A, Y346M and Y346F) were studied, cancelling the electron donating character of this residue. The ultrafast flavin photoreduction observed in WT and C53A is here effectively inhibited but slower, secondary excited-state quenching channels are detected (4.0, 100 and 1600 ps in Y346A). No major differences are seen between the different mutants. Since *BsTrmFO* does not bear the W_{214} residue invoked to play the role of secondary electron donor in *TtTrmFO*,¹⁹ two alternative hypotheses are invoked to explain the observed decays. It may first be supposed that W_{286} , situated at 8.2 Å from FAD, is capable of reducing the excited flavin. It is however difficult to explain how this sole residue, which lies in a non-flexible region of the protein, would account for all the decay components. Without ruling out the possibility that this

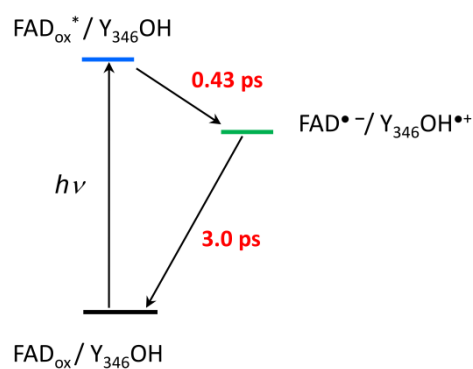
quenching by W_{286} accounts for one of the observed decays, we tentatively favor the idea that the Y_{346} mutations destabilize the anchoring of the isoalloxazine ring¹⁴ and allow a relatively large conformational heterogeneity of TrmFO's active site. This would in turn create a distribution of isoalloxazine-adenine distance, the adenine moiety playing the role of quencher as in the stacked configuration of FAD_{ox} in solution.³⁹ The conformational sampling of FAD would therefore suitably explain a part of the multiexponential decay.

Overall, the first outcome of this study is a clear support for the π - π stacking and H-bond coupling mechanism in the control of TrmFO's active site dynamics, required for competent orientation of the reactive centers during catalysis. Secondly, the fact that short-lived $FAD^{\bullet-}/YOH^{\bullet+}$ photoproduct is stabilized by both mesophilic and thermophilic orthologous enzymes indicates that this photochemical property is an inherent peculiarity of TrmFO's active site making this family of flavoprotein a suitable model for future investigations of $YOH^{\bullet+}$ reactivity.

Tables and Figures

Table 1. Time constants of the global multiexponential fit of the transient absorption spectra of the five studied variants of *BsTrmFO* (WT, C53A, Y346A, Y346M and Y346F), obtained upon excitation at 475 nm. Fit errors (σ) are indicated after the \pm sign. The coefficient of determination (R^2) characterizing the quality of the fit is given in the last column.

Variant	τ_1 (ps)	τ_2 (ps)	τ_3 (ps)	τ_4 (ps)	τ_5 (ps)	R^2
WT	0.38 ± 0.03	1.15 ± 0.1	4.1 ± 0.3	43 ± 8	700 ± 50	0.99972
C53A	0.30 ± 0.02	1.0 ± 0.1	3.0 ± 0.3	9.3 ± 1.4		0.99986
Y346A	4.0 ± 0.3	100 ± 10	1600 ± 100			0.99971
Y346M	4.2 ± 0.2	93 ± 6	1420 ± 50			0.99985
Y346F	3.9 ± 0.3	89 ± 7	1650 ± 60			0.99982



Scheme 1. Simplified reaction scheme of *BsTrmFO/C53A* (only the main electron transfer reactions are represented).

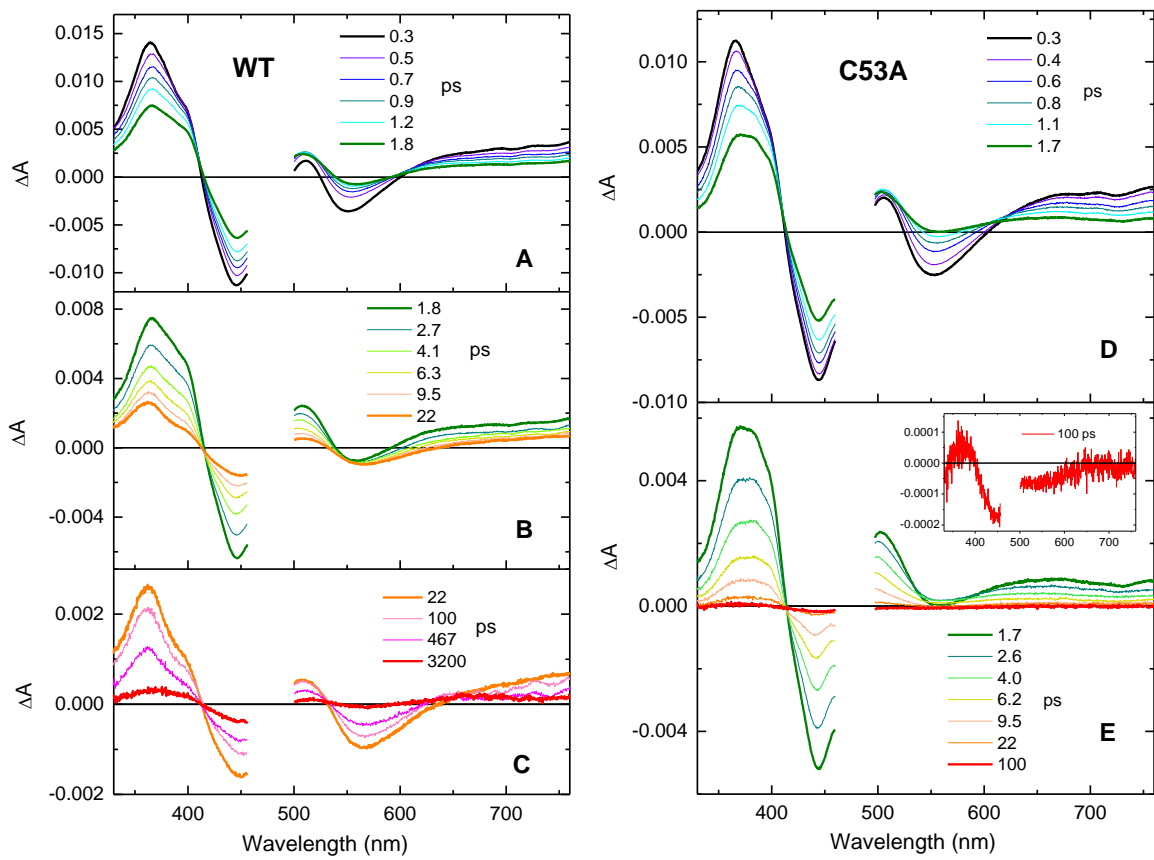


Figure 1. Isotropic transient spectra of the of wild-type *BstTrmFO* (A-C) and of its C53A mutant (D-E) at selected pump-probe delays, after excitation at 475 nm.

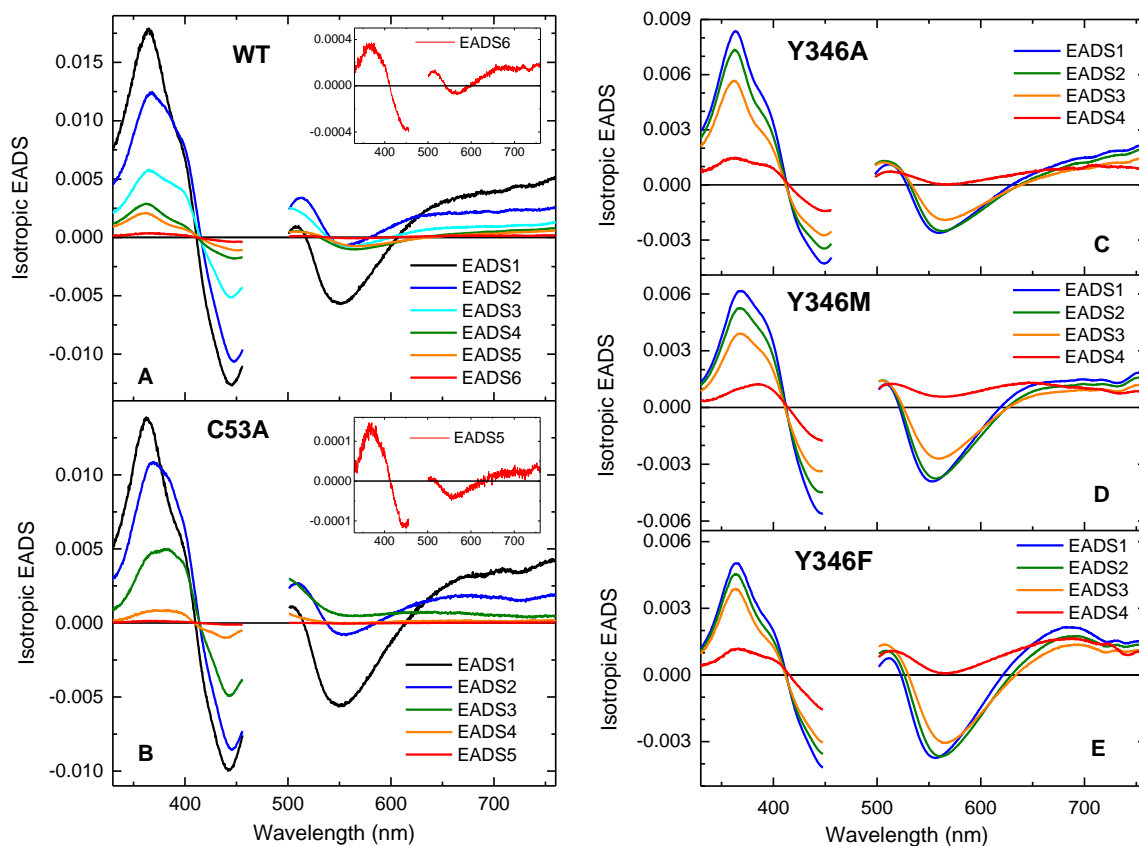


Figure 2. Isotropic EADS deduced from the global fit of the transient absorption spectra of WT (A), C53A (B), Y346A (C), Y346M (D) and Y346F (E), after excitation at 475 nm. See corresponding time constants in Table 1.

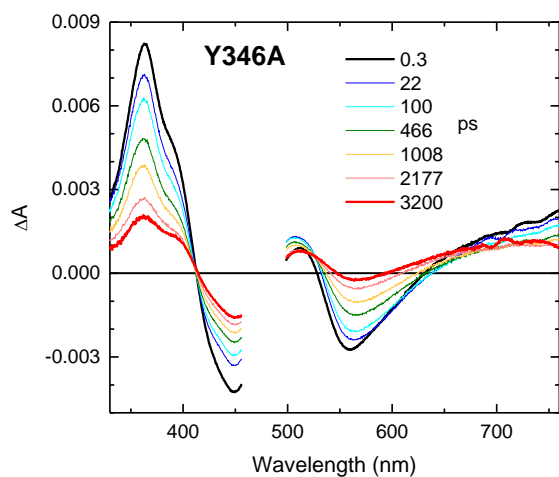


Figure 3. Isotropic transient spectra of the Y346A mutant of *BsTrmFO* at selected pump-probe delays, after excitation at 475 nm.

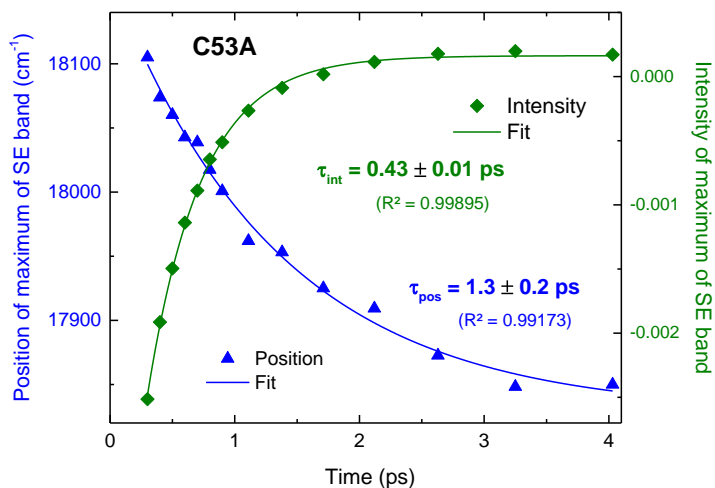


Figure 4. Tracking of the spectral position (left y-axis) and the intensity (right y-axis) of the maximum of the SE band of C53A, after excitation at 475 nm, as a function of time. To increase the precision of the readings, the SE bands were first locally fitted by exponentially modified Gaussians. The data points were then independently fitted by a single exponential decay ($y = y_0 + a e^{-t/\tau}$).

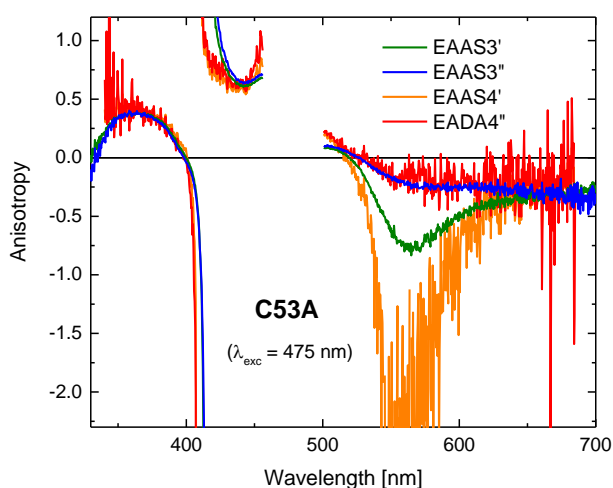


Figure 5. Correction of EAAS3 and EAAS4 in the case of C53A with excitation at 475 nm. EAAS' are the anisotropy spectra deduced from the polarized EADS' (Equation 3); EAAS'' are further deduced from EADS'' (Equation 4).

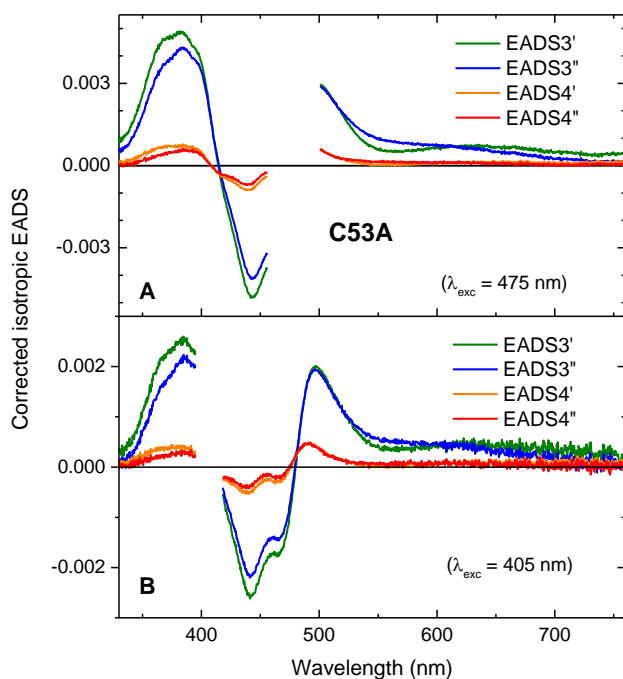


Figure 6. Correction of EADS3 and EADS4 in the case of C53A with excitation at 475 nm (A) and 405 nm (B). EADS' and EADS'' are deduced from Equations 3 and 4 with the same choice of α parameters as in Figure 5.

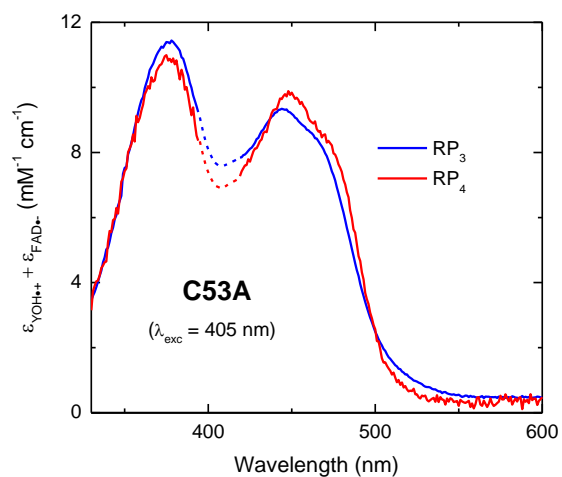


Figure 7. Molar absorption coefficient spectrum of the $FAD^{\bullet-}/Y_{346}OH^{\bullet+}$ radical pair, as extracted with Equation 6 from EADS3'' (RP₃) and from EADS4'' (RP₄) of C53A with excitation at 405 nm. The region in dotted line corresponds to linearly interpolated EADS'' in the masked region of pump scattering.

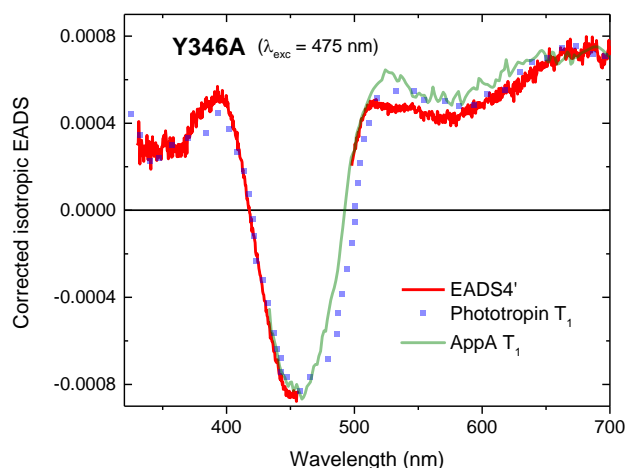


Figure 8. Correction of EADS4 in the case of Y346A with excitation at 475 nm. EADS'4 (red line) is deduced from Equation 8: α was chosen so as to let EADS'4 resemble the transient absorption spectra of the triplet state of the phototropin from *Avena sativa* (LOV2 domain)⁷⁶ (blue squares) and AppA from *Rhodobacter sphaeroides* (BLUF domain)⁷⁵ (green line).

CONFLICT OF INTERESTS

There are no conflicts to declare.

ACKNOWLEDGEMENTS

This work was supported by French State Program "Investissements d'Avenir" (ANR-15-CE11-0004-01).

REFERENCES

1. C. T. Walsh and T. A. Wencewicz, *Nat. Prod. Rep.*, 2013, **30**, 175-200.
2. V. Piano, B. A. Palfey and A. Mattevi, *Trends Biochem. Sci.*, 2017, **42**, 457-469.
3. Y. T. Kao, C. Saxena, T. F. He, L. J. Guo, L. J. Wang, A. Sancar and D. P. Zhong, *J. Am. Chem. Soc.*, 2008, **130**, 13132-13139.
4. V. Nandwana, I. Samuel, G. Cooke and V. M. Rotello, *Acc. Chem. Res.*, 2013, **46**, 1000-1009.
5. L. Fruk, C.-H. Kuo, E. Torres and C. M. Niemeyer, *Angew. Chem. Int. Ed.*, 2009, **48**, 1550-1574.
6. J. Urbonavicius, S. Skouloubris, H. Myllykallio and H. Grosjean, *Nucleic Acids Res.*, 2005, **33**, 3955-3964.
7. H. Nishimasu, R. Ishitani, K. Yamashita, C. Iwashita, A. Hirata, H. Hori and O. Nureki, *Proc. Natl. Acad. Sci. USA*, 2009, **106**, 8180-8185.
8. R. Yamagami, K. Yamashita, H. Nishimasu, C. Tomikawa, A. Ochi, C. Iwashita, A. Hirata, R. Ishitani, O. Nureki and H. Hori, *J. Biol. Chem.*, 2012, **287**, 42480-42494.
9. D. Hamdane, H. Grosjean and M. Fontecave, *J. Mol. Biol.*, 2016, **428**, 4867-4881.
10. D. Hamdane, V. Guerineau, S. Un and B. Golinelli-Pimpaneau, *Biochemistry*, 2011, **50**, 5208-5219.

11. D. Hamdane, M. Argentini, D. Cornu, H. Myllykallio, S. Skouloubris, G. Hui-Bon-Hoa and B. Golinelli-Pimpaneau, *J. Biol. Chem.*, 2011, **286**, 36268-36280.
12. D. Hamdane, M. Argentini, D. Cornu, B. Golinelli-Pimpaneau and M. Fontecave, *J. Am. Chem. Soc.*, 2012, **134**, 19739-19745.
13. D. Hamdane, E. Bruch, S. Un, M. Field and M. Fontecave, *Biochemistry*, 2013, **52**, 8949-8956.
14. D. Hamdane, C. Bou-Nader, D. Cornu, G. Hui-Bon-Hoa and M. Fontecave, *Biochemistry*, 2015, **54**, 4354-4364.
15. H. Hori, *Front. Gen.*, 2014, **5**.
16. C. Bou-Nader, D. Cornu, V. Guerineau, T. Fogeron, M. Fontecave and D. Hamdane, *Angew. Chem. Int. Ed.*, 2017, **56**, 12523-12527.
17. T. V. Mishanina, L. Yu, K. Karunaratne, D. Mondal, J. M. Corcoran, M. A. Choi and A. Kohen, *Science*, 2016, **351**, 507-510.
18. H. Myllykallio, P. Sournia, A. Heliou and U. Liebl, *Front. Microbiol.*, 2018, **9**.
19. L. Nag, P. Sournia, H. Myllykallio, U. Liebl and M. H. Vos, *J. Am. Chem. Soc.*, 2017, **139**, 11500-11505.
20. N. Mataga, H. Chosrowjan, Y. Shibata, F. Tanaka, Y. Nishina and K. Shiga, *J. Phys. Chem. B*, 2000, **104**, 10667-10677.
21. D. P. Zhong and A. H. Zewail, *Proc. Natl. Acad. Sci. USA*, 2001, **98**, 11867-11872.
22. N. Mataga, H. Chosrowjan, S. Taniguchi, F. Tanaka, N. Kido and M. Kitamura, *J. Phys. Chem. B*, 2002, **106**, 8917-8920.
23. M. Gauden, J. S. Grinstead, W. Laan, I. H. M. van Stokkum, M. Avila-Perez, K. C. Toh, R. Boelens, R. Kaptein, R. van Grondelle, K. J. Hellingwerf and J. T. M. Kennis, *Biochemistry*, 2007, **46**, 7405-7415.
24. Y. T. Kao, C. Tan, S. H. Song, N. Ozturk, J. Li, L. J. Wang, A. Sancar and D. P. Zhong, *J. Am. Chem. Soc.*, 2008, **130**, 7695-7701.
25. K. Brettel and M. Byrdin, *Curr. Opin. Struct. Biol.*, 2010, **20**, 693-701.
26. D. Immeln, A. Weigel, T. Kottke and J. L. Perez Lustres, *J. Am. Chem. Soc.*, 2012, **134**, 12536-12546.
27. K. Lugsanangarm, S. Pianwanit, A. Nueangaudom, S. Kokpol, F. Tanaka, N. Nunthaboot, K. Ogino, R. Takagi, T. Nakanishi, M. Kitamura, S. Taniguchi and H. Chosrowjan, *J. Photochem. Photobiol. A*, 2013, **268**, 58-66.
28. F. Tanaka, K. Lugsanangarm, N. Nunthaboot, A. Nueangaudom, S. Pianwanit, S. Kokpol, S. Taniguchi and H. Chosrowjan, *Phys. Chem. Chem. Phys.*, 2015, **17**, 16813-16825.
29. K. Lugsanangarm, A. Nueangaudom, S. Kokpol, S. Pianwanit, N. Nunthaboot, F. Tanaka, S. Taniguchi and H. Chosrowjan, *J. Photochem. Photobiol. A*, 2015, **306**, 66-79.
30. N. Nunthaboot, K. Lugsanangarm, A. Nueangaudom, S. Pianwanit, S. Kokpol, F. Tanaka, S. Taniguchi, H. Chosrowjan, T. Nakanishi and M. Kitamura, *J. Photochem. Photobiol. A*, 2016, **326**, 60-68.
31. S. P. Laptinok, L. Bouzhir-Sima, J.-C. Lambry, H. Myllykallio, U. Liebl and M. H. Vos, *Proc. Natl. Acad. Sci. USA*, 2013, **110**, 8924-8929.
32. W. T. Dixon and D. Murphy, *J. Chem. Soc. Faraday Trans. II*, 1976, **72**, 1221-1230.
33. K. Lugsanangarm, S. Pianwanit, S. Kokpol, F. Tanaka, H. Chosrowjan, S. Taniguchi and N. Mataga, *J. Photochem. Photobiol. A*, 2011, **219**, 32-41.
34. J. Pan, M. Byrdin, C. Aubert, A. P. M. Eker, K. Brettel and M. H. Vos, *J. Phys. Chem. B*, 2004, **108**, 10160-10167.
35. Z. Y. Liu, C. Tan, X. M. Guo, J. Li, L. J. Wang, A. Sancar and D. P. Zhong, *Proc. Natl. Acad. Sci. USA*, 2013, **110**, 12966-12971.
36. R. Martin, F. Lacombat, A. Espagne, N. Dozova, P. Plaza, J. Yamamoto, P. Muller, K. Brettel and A. de la Lande, *Phys. Chem. Chem. Phys.*, 2017, **19**, 24493-24504.
37. D. Hamdane, S. Skouloubris, H. Myllykallio and B. Golinelli-Pimpaneau, *Protein Expr. Purif.*, 2010, **73**, 83-89.
38. R. J. Stanley and H. Jang, *J. Phys. Chem. A*, 1999, **103**, 8976-8984.

39. J. Brazard, A. Usman, F. Lacombat, C. Ley, M. M. Martin and P. Plaza, *J. Phys. Chem. A*, 2011, **115**, 3251-3262.
40. J. Brazard, A. Usman, F. Lacombat, C. Ley, M. M. Martin, P. Plaza, L. Mony, M. Heijde, G. Zabulon and C. Bowler, *J. Am. Chem. Soc.*, 2010, **132**, 4935-4945.
41. A. Yoshimura, M. Z. Hoffman and H. Sun, *J. Photochem. Photobiol. A*, 1993, **70**, 29-33.
42. M. Byrdin, V. Thiagarajan, S. Villette, A. Espagne and K. Brettel, *Rev. Sci. Instr.*, 2009, **80**, 043102.
43. K. Ekvall, P. van der Meulen, C. Dhollande, L. E. Berg, S. Pommeret, R. Naskrecki and J. C. Mialocq, *J. Appl. Phys.*, 2000, **87**, 2340-2352.
44. M. Byrdin, S. Villette, A. Espagne, A. P. M. Eker and K. Brettel, *J. Phys. Chem. B*, 2008, **112**, 6866-6871.
45. E. R. Henry and J. Hofrichter, *Methods Enzymol.*, 1992, **210**, 129-193.
46. I. H. M. van Stokkum, S. L. Delmar and R. van Grondelle, *Biochim. Biophys. Acta Bioenerg.*, 2004, **1657**, 82-104.
47. M. Gauden, I. H. M. van Stokkum, J. M. Key, D. C. Luehrs, R. Van Grondelle, P. Hegemann and J. T. M. Kennis, *Proc. Natl. Acad. Sci. USA*, 2006, **103**, 10895-10900.
48. J. P. Hoben, C. E. Lubner, M. W. Ratzloff, G. J. Schut, D. M. N. Nguyen, K. W. Hempel, M. W. W. Adams, P. W. King and A.-F. Miller, *J. Biol. Chem.*, 2017, **292**, 14039-14049.
49. A. Weigel, A. Dobryakov, B. Klaumuenzer, M. Sajadi, P. Saalfrank and N. P. Ernsting, *J. Phys. Chem. B*, 2011, **115**, 3656-3680.
50. F. Lacombat, A. Espagne, N. Dozova, P. Plaza, E. Ignatz, S. Kiontke and L.-O. Essen, *Phys. Chem. Chem. Phys.*, 2018, **20**, 25446-25457.
51. R. A. Marcus and N. Sutin, *Biochim. Biophys. Acta*, 1985, **811**, 265-322.
52. C. C. Page, C. C. Moser, X. X. Chen and P. L. Dutton, *Nature*, 1999, **402**, 47-52.
53. C. Aubert, P. Mathis, A. P. M. Eker and K. Brettel, *Proc. Natl. Acad. Sci. USA*, 1999, **96**, 5423-5427.
54. B. Giese, M. Wang, J. Gao, M. Stoltz, P. Müller and M. Graber, *J. Org. Chem.*, 2009, **74**, 3621-3625.
55. D. Nohr, S. Franz, R. Rodriguez, B. Paulus, L. O. Essen, S. Weber and E. Schleicher, *Biophys. J.*, 2016, **111**, 301-311.
56. P. Changenet-Barret, C. T. Choma, E. F. Gooding, W. F. DeGrado and R. M. Hochstrasser, *J. Phys. Chem. B*, 2000, **104**, 9322-9329.
57. S. K. Pal, J. Peon and A. H. Zewail, *Proc. Natl. Acad. Sci. USA*, 2002, **99**, 1763-1768.
58. C.-W. Chang, T.-F. He, L. Guo, J. A. Stevens, T. Li, L. Wang and D. Zhong, *J. Am. Chem. Soc.*, 2010, **132**, 12741-12747.
59. S. Mondal, S. Mukherjee and B. Bagchi, *J. Chem. Phys.*, 2017, **147**, 11.
60. A. Szilagyi and P. Zavodszky, *Structure*, 2000, **8**, 493-504.
61. F. Tanaka, H. Chosrowjan, S. Taniguchi, N. Mataga, K. Sato, Y. Nishina and K. Shiga, *J. Phys. Chem. B*, 2007, **111**, 5694-5699.
62. M. Kundu, T.-F. He, Y. Lu, L. Wang and D. Zhong, *J. Phys. Chem. Lett.*, 2018, **9**, 2782-2790.
63. F. Lacombat, P. Plaza, M. A. Plamont and A. Espagne, *J. Phys. Chem. Lett.*, 2017, **8**, 1489-1495.
64. V. Massey and G. Palmer, *Biochemistry*, 1966, **5**, 3181-3189.
65. B. Liu, H. Liu, D. Zhong and C. Lin, *Curr. Opin. Plant Biol.*, 2010, **13**, 578-586.
66. A. Berndt, T. Kottke, H. Breitzkreuz, R. Dvorsky, S. Hennig, M. Alexander and E. Wolf, *J. Biol. Chem.*, 2007, **282**, 13011-13021.
67. V. E. Zubarev and O. Brede, *Acta Chem. Scand.*, 1997, **51**, 224-228.
68. K. Kesper, F. Diehl, J. G. G. Simon, H. Specht and A. Schweig, *Chem. Phys.*, 1991, **153**, 511-517.
69. T. A. Gadosy, D. Shukla and L. J. Johnston, *J. Phys. Chem. A*, 1999, **103**, 8834-8839.
70. P. A. W. van den Berg, K. A. Feenstra, A. E. Mark, H. J. C. Berendsen and A. Visser, *J. Phys. Chem. B*, 2002, **106**, 8858-8869.
71. H. Chosrowjan, S. Taniguchi, N. Mataga, F. Tanaka and A. Visser, *Chem. Phys. Lett.*, 2003, **378**, 354-358.

72. A. Penzkofer, L. Endres, T. Schiereis and P. Hegemann, *Chem. Phys.*, 2005, **316**, 185-194.
73. J. T. M. Kennis, S. Crosson, M. Gauden, I. H. M. van Stokkum, K. Moffat and R. van Grondelle, *Biochemistry*, 2003, **42**, 3385-3392.
74. A. Losi, E. Polverini, B. Quest and W. Gärtner, *Biophys. J.*, 2002, **82**, 2627-2634.
75. M. Gauden, S. Yeremenko, W. Laan, I. H. M. van Stokkum, J. A. Ihalainen, R. van Grondelle, K. J. Hellingwerf and J. T. M. Kennis, *Biochemistry*, 2005, **44**, 3653-3662.
76. T. E. Swartz, S. B. Corchnoy, J. M. Christie, J. W. Lewis, I. Szundi, W. R. Briggs and R. A. Bogomolni, *J. Biol. Chem.*, 2001, **276**, 36493-36500.